Ratchet current in nontwist Hamiltonian systems

Cite as: Chaos **30**, 093141 (2020); https://doi.org/10.1063/5.0022073
Submitted: 17 July 2020 . Accepted: 10 September 2020 . Published Online: 23 September 2020

Michele Mugnaine, Antonio M. Batista, Iberê L. Caldas, José D. Szezech, and Ricardo L. Viana

Ratchet current in nontwist Hamiltonian systems

Cite as: Chaos **30**, 093141 (2020); doi: 10.1063/5.0022073
Submitted: 17 July 2020 · Accepted: 10 September 2020 ·
Published Online: 23 September 2020

Michele Mugnaine,[1] Antonio M. Batista,[2,3,4] Iberê L. Caldas,[4] José D. Szezech, Jr.,[2,3,a)] and Ricardo L. Viana[1]

AFFILIATIONS

[1]Department of Physics, Federal University of Paraná, 80060-000 Curitiba, PR, Brazil
[2]Department of Mathematics and Statistics, State University of Ponta Grossa, 84030-900 Ponta Grossa, PR, Brazil
[3]Graduate in Science Program - Physics, State University of Ponta Grossa, 84030-900 Ponta Grossa, PR, Brazil
[4]Institute of Physics, University of São Paulo, 05508-900 São Paulo, SP, Brazil

[a)]**Author to whom correspondence should be addressed:** jdsjunior@uepg.br

ABSTRACT

Non-monotonic area-preserving maps violate the twist condition locally in phase space, giving rise to shearless invariant barriers surrounded by twin island chains in these regions of phase space. For the extended standard nontwist map, with two resonant perturbations with distinct wave numbers, we investigate the presence of such barriers and their associated island chains and compare our results with those that have been reported for the standard nontwist map with only one perturbation. Furthermore, we determine in the control parameter space the existence of the shearless barrier and the influence of the additional wave number on this condition. We show that only for odd second wave numbers are the twin island chains symmetrical. Moreover, for even wave numbers, the lack of symmetry between the chains of twin islands generates a ratchet effect that implies a directed transport in the phase space.

The collective motion of many trajectories is a subject of great interest in many areas, in particular, how transport occurs and changes for specific conditions. The ratchet models are an outstanding description to explain the transport phenomena in spatially periodic systems without a directed force. The ratchet models have been considered in many applications, for instance, atoms in waves of light, turbulent plasmas, cold atoms, molecular motors, and others. In this work, we study the ratchet transport in a non-monotonic system called Extended Standard Nontwist Map (ESNM). The ESNM is a modified version of the Standard Nontwist Map known for describing transport in reverse shear and barrier breaking systems. The extended version produces new features such as unbalanced stickiness and unbiased transport. We investigate the parameter space in detail to identify the breakup of the transport barrier and the emergence of a directed ratchet transport. In addition, the parameters for which the directed transport is null, negative, or positive are presented.

I. INTRODUCTION

In dynamical systems, the characterization of transport plays an important role in many areas of research since it helps us to understand the movement of groups of chaotic trajectory. The study of transport in Hamiltonian systems is well established and based on the Kolmogorov–Arnold–Moser (KAM) theorem.[1] When the last torus is broken, the last barrier disappears and, as a consequence, the whole chaotic sea in the phase space is available for the chaotic solution to visit. The remnants of the last KAM tori can act as a partial barrier and limit the motion of irregular system components.[1,2] The properties and transport mechanism of the standard map were studied by MacKay *et al.*[2] and the Cantor sets, named cantori, were responsible for the partial restraint to the chaotic trajectories.

Transport applications are relevant to atmospheric and oceanic problems, where the particle transport in geophysical flows is important for plasmas and accelerators, where particles are lost, for wave heating rates in plasmas, chemical reactions, and many other physical, biological, and social problems.[2–4]

Recently, a new feature was observed in the conservative transport phenomenon: a preferential direction for the transport in the phase space without external bias, the so-called Hamiltonian ratchets.[5] The ratchet effect is defined by the emergence of a directed current, or ratchet current, which is characterized by the directed motion of the chaotic trajectories without a directed force.[4,6–10] The ratchet study is motivated by its application in atoms in waves of light,[7] turbulent plasmas,[11,12] cold atoms,[13] molecular motors,[14] and other examples.

In previous works, it was demonstrated that the ratchet effect is a consequence of a spatial and/or temporal symmetry breaking of the system. Since, by definition, a directed force is not present, the breaking of symmetries is responsible for the transport. Wang *et al.*[15] studied the ratchet effect on the extension of the standard map, where the space and time symmetry is broken by the introduction of unevenly spaced and phase shifted kicks. As a consequence, a nonzero classical current, represented by a nonzero first moment, is identified.[15] Gong and Brumer[5] examined the scenario of directed transport in the modified kicked rotor system where the spatial symmetry is broken by a second kicking field. They showed that due to the spatial symmetry, regular islands immersed in the chaotic sea have partners in the Poincaré section. Thus, when the spatial symmetry is broken, the structure of partner islands is also broken and the chaotic trajectories tend to move in a specific direction.[5]

The twist maps have already been used to study the ratchet effect. They satisfied the twist condition globally and the KAM theorem can be used to study the barriers in the system. However, the ratchet effect has not yet been reported in nontwist maps. A nontwist system violates the twist condition on an invariant curve in the phase space, the shearless curve.[16] The standard nontwist map (SNM) was introduced by del Castillo-Negrete and Morrison.[16] The SNM is a simple nontwist system that presents particular features: the winding number profile is non-monotonic, the scenario of twin islands, reconnection, and collision of regular orbits.[16–19] In addition, transport in nontwist maps is peculiar due to the presence of a robust shearless barrier surrounded by chains of twin islands. The development of efficient algorithms to determine the values for which values of the parameters' non-twist curves breakdown is still a developing question; in Ref. 20, it was determined the domain of existence of the non-twist curves for a two parameter family of quadratic standard maps.

The SNM is a symmetric map and the inherent symmetry of the system can be preserved or broken with the addition of a new perturbation. In this paper, we study the effects and consequences of the breaking symmetry in the phase space transport for another nontwist map. Our object of study is the extended standard nontwist map (ESNM) introduced by Portela *et al.*[21] as a nontwist map with two distinct resonant perturbations due to resonant external coils in tokamaks. We determine in the control parameter space the existence of the shearless barrier and the influence of the second resonant perturbation on this condition. We also show the presence of directed transport, the so-called ratchet effect, when the symmetry is broken, in agreement with previously cited works. The novelty in our results is the demonstration of the broken twin scenario, where there is no more correspondence between the chains of twin islands, once the symmetry is broken. This scenario leads to unbalanced stickiness and unbiased transport. We also emphasize the modification in the transport barriers due to the symmetry breaking. We show that, for an asymmetric case, the parameter space for the existence of the barrier can be considered as a disjoint set, for some cases, and has a nontrivial structure.

Our paper is organized as follows: in Sec. II, we introduce the ESNM, as well as the consequences of the new perturbation in the phase space and in the symmetry of the system. In Sec. III, we provide the parameter spaces related to the existence of a barrier in the phase space for the extended map, as well as a method for identifying the transport barriers for the asymmetric cases. Section IV is dedicated to the directed transport discussion, where we define our ratchet behavior and identify the preferential direction for the chaotic trajectories. In Sec. V, we present our conclusions.

II. EXTENDED STANDARD NONTWIST MAP AND THE SYMMETRY BREAKUP

The nontwist version of the extended standard map is defined in Refs. 21 and 22 as

$$\begin{aligned} y_{n+1} &= y_n - b\sin(2\pi x_n) - c\sin(2\pi m x_n), \\ x_{n+1} &= x_n + a(1 - y_{n+1}^2) \mod 1, \end{aligned} \tag{1}$$

where a, b, and c are real parameters and $m \in \mathbb{Z}$. We consider $x \in [0, 1)$ and $y \in \mathbb{R}$. Map (1) is called extended standard nontwist map (ESNM) or two-frequency standard nontwist map.[22] The parameter a is the profile parameter and b and c are the amplitudes of different source perturbations.[21] If $c = 0$, we recover the standard nontwist map (SNM) proposed by del Castillo-Negrete and Morrison.[17] On the other hand, the extended twist standard map was studied by Greene *et al.*[23] from the perspective of fixed points with high periods and a renormalization approach.

In order to investigate the role of the new perturbation $c\sin(2\pi m x_n)$, we construct the phase spaces for four cases of m, $a = 0.805$, $b = 0.597$, and $c = 0.005$. The phase spaces for $m = 1, 2, 3$, and 4 are shown in Fig. 1.

In Fig. 1, we have that all the phase spaces are composed of a chaotic sea (black dots) and two chains of islands: one composed of green dots and others of blue dots. The colored curves are the symmetry lines for the map (see Sec. III). For an odd m, $m = 1$ at (a)–(c) and $m = 3$ at (g)–(i), the twin island chain scenario is observed in the phase space, where the blue and the green islands are similar [magnification in Figs. 1(b) and 1(c) and 1(h) and 1(i)]. The twin islands have the same size, and the inner curves' bifurcation happens at the same point for both chains. In this case, the islands of each chain highlighted in the magnifications are corresponding twins, namely, the green island is the symmetrical transformation of the blue one. However, for even m, this scenario is modified so that the two chains of islands are not twins. For $m = 2$, Figs. 1(d)–1(f), the blue islands are bigger than the green ones and the inner structure is different. A similar situation happens for $m = 4$ [Figs. 1(j)–1(l)], the islands have different sizes and shapes, and we see an island chain structure around the blue islands and not around the green islands.

In Fig. 1, for even m, we see the breakup of the twin island chain scenario, consequently, the breakup of a symmetry structure of the system. Can we say that the map is asymmetric? A map M is said to be symmetric over a transformation T if M satisfies the $TM = MT$ relationship. The standard nontwist map, $c = 0$ in (1), is a symmetric map over the symmetry transformation,[16]

$$T = \left(x \pm \frac{1}{2}, -y\right). \tag{2}$$

This transformation allows us to find two regular orbits with the same winding number. We find a solution with winding number ω applying the transformation (2) and find another orbit with the

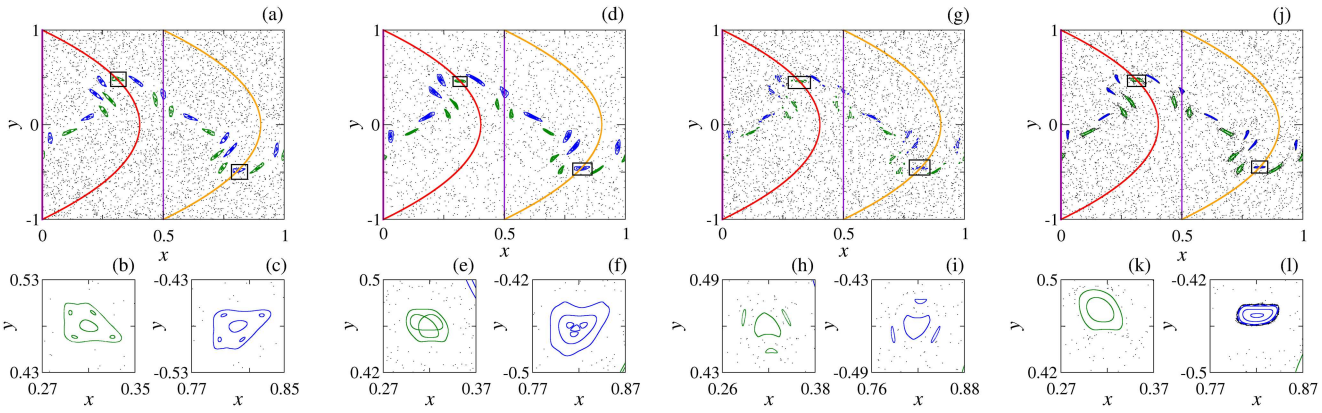

FIG. 1. Phase spaces and their respective amplifications of the islands $a = 0.805$, $b = 0.597$, $c = 0.005$, and (a)–(c) $m = 1$, (d)–(f) $m = 2$, (g)–(i) $m = 3$, and (j)–(l) $m = 4$. The symmetry lines are represented by the colored curves: S_0 in magenta, S_1 in red, S_2 in violet, and S_4 in orange (more details in Sec. III).

same ω. Thus, an island in the blue chain with a winding number ω and its twin in the green chain (1) are related by Eq. (2). To build the two island chains in Figs. 1(a) and 1(g), we find an initial condition, which generates the blue island chain and applies the symmetry transformation to find the initial condition for the green island chain.

If we apply the transformation (2) and the ESNM (1) in the $TM = MT$ relationship, we find the identities

$$\begin{aligned}(x \pm 1/2) + a(1 - y_{n+1}^2) &= [x + a(1 - y_{n+1}^2)] \pm 1/2,\\ -y + b\sin(2\pi x) + c(-1)^{m+1}\sin(2\pi mx) &\\ = -y + b\sin(2\pi x) + c\sin(2\pi mx),&\end{aligned} \tag{3}$$

where the second identity is true only if m is odd. Thus, for even m, the map is asymmetric as shown in Figs. 1(d)–1(f) and 1(j)–1(l).

The twin island chain is a structure in nontwist systems[24–27] with influence and effect on transport through the phase space. Due to the different island scenarios for different values of m, the motion of the chaotic trajectories in the phase space is an interesting point to study. A simple analysis can be done by the average of y (the momentum) over time. To obtain this average, we randomly choose a large number of chaotic initial conditions, over $y = 0$, iterate and calculate the spatial average $\langle y\rangle$ for each iteration n. The average $\langle y\rangle$ for $a = 0.805$, $b = 0.597$, $c = 0.005$, and different values of m are shown in Fig. 2.

The space average of y for odd m is close to zero during all iterations, as shown in Fig. 2(a) for $m = 1$ (blue line) and for $m = 3$ (green line). Therefore, the orbits tend to go up and downward equally in the phase space. For even m, this equality does not occur, and we see a tendency of the average to always be negative during all iterations, as shown in Fig. 2(a) for $m = 2$ (red line) and $m = 4$ (orange line). According to Gong and Brumer,[5] $\langle y\rangle$ represents the classical net current and once $\langle y\rangle \neq 0$, we observe a Hamiltonian ratchet effect for even values of m. The ratchet effects are evidenced in the phase space in Figs. 2(c) and 2(e), where we plot the first $n = 1000$ iterations for 100 initial conditions over $y = 0$ (green line) in the chaotic sea. The ratchet effects are exhibited in Figs. 2(c) and 2(e) for $m = 2$ and $m = 4$, respectively, where we observe an asymmetric concentration of points around the island chains. In both cases, the concentration is higher around the upper chain island, in accordance with the negative space average shown in Fig. 2(a). The high density of points around the upper islands indicates an unbiased stickiness where the orbits that go upward got stuck in this region, while the orbits that go downward do not find any trap or obstacle in their path. In this way, we have a preferential direction and a current in the phase space. For the symmetric cases, $m = 1$ and $m = 3$, shown in Figs. 2(b) and 2(d), we see that the concentration of points is symmetric, namely, the orbits get stick whether they go upward or downward.

From the phases spaces in Fig. 1, the net current in Fig. 2(a), and the chaotic trajectories also shown in Figs. 2(b)–2(e), we conclude that the symmetry breaking for even m generates directed transport. The ratchet effects observed in our system are also similar to the directed transport, characterized for a nonzero value of $\langle y\rangle$ in the extended standard map with spatial and temporal asymmetry, which was examined by Cheon.[28] The novelty in our result is the observation of directed transport for nontwist systems and the explanation of this scenario is related to the particular properties of these systems, the broken twin islands scenario. The unbalanced and asymmetric stickiness scenario around the two chains of islands are responsible for the ratchet effect in these phase spaces.

III. PARAMETER SPACE

As shown by Wurm and Martini,[22] the ESNM map M_E can be decomposed in two involutions as $M_E = I_1 \circ I_0$, where

$$\begin{aligned}I_0(x,y) &= (-x, y - b\sin(2\pi x) - c\sin(2\pi mx)),\\ I_1(x,y) &= (-x + a(1-y^2), y),\end{aligned} \tag{4}$$

and the involution satisfies the relations $M_E^{-1} = I_i^{-1} M_E I_i$ and $I_i^2 = \mathbb{I}$, for $i = 0, 1$, where $\mathbb{I}$ is the identity. The symmetry lines are one-dimensional invariant sets composed by the points $\mathbf{x} = (x, y)$ that are solutions for the relations $I_{0,1}\mathbf{x} = \mathbf{x}$.[16] For the ESNM, we

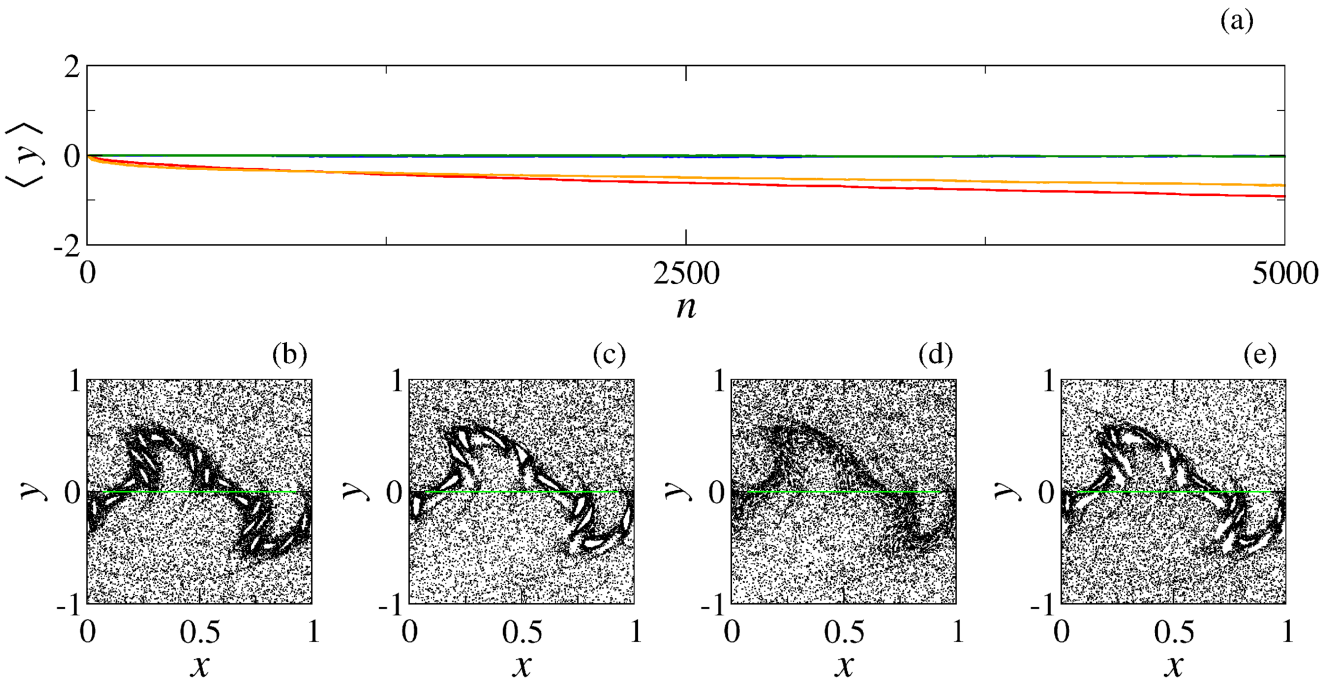

FIG. 2. (a) Ensemble average of y in terms of 10^6 initial conditions randomly distributed on $y = 0$, the green line, at $n = 0$. We choose the same parameters as in Fig. 1 and each color represent a value of m: blue ($m = 1$), red ($m = 2$), green ($m = 3$), and orange ($m = 4$). The phase spaces for the first $n = 1000$ iterations of 100 chaotic initial conditions uniformly distributed over $y = 0$ (green line) and (b) $m = 1$, (c) $m = 2$, (d) $m = 3$, and (e) $m = 4$.

have the following symmetry lines:

$$S_0 = \{(x, y)|x = 0\},$$
$$S_1 = \left\{(x, y)|x = \frac{a(1 - y^2)}{2}\right\}. \quad (5)$$

The transformation of symmetry is necessary to determine the indicator points (IPs) that indicate the presence of the shearless curve.[29,30] The indicator points allow us to study the reconnection of twin island chains and help us to identify the transition to global chaos.[30] The IP $\mathbf{z}_i$ are solutions of $I_i\mathbf{z}_i = T\mathbf{z}_i$,[30] where I_i are the involution (4) and T is the symmetry transformation (2). Since the symmetry transformation is valid only for odd m, as shown in

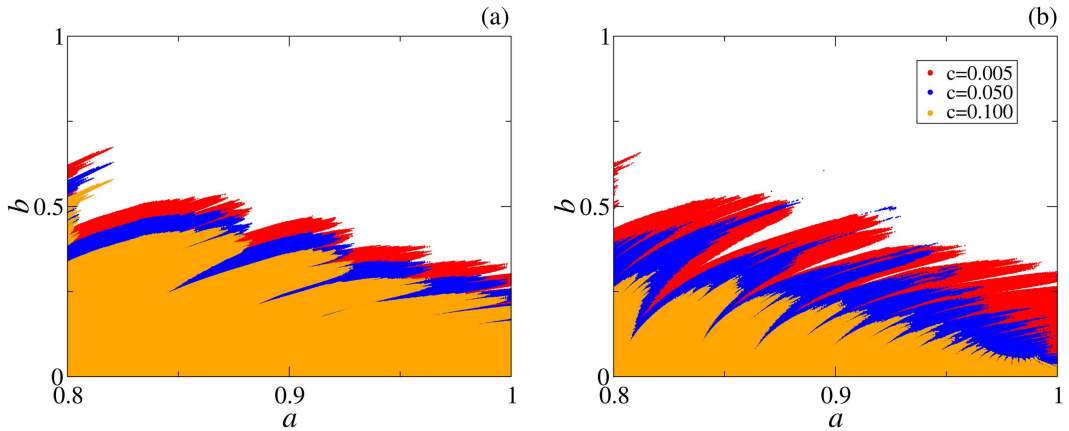

FIG. 3. Parameter spaces for the existence of the shearless curve for odd m and different values of c. In (a), we see the parameter spaces for $m = 1$ and in (b) for $m = 3$. The parameter spaces are superimposed on each other.

Eq. (3), the indicator points can be defined as $m = 1$ and $m = 3$. Therefore, the indicator points for ESNM with odd m are given by

$$\mathbf{z_0}^{(0,1)} = \left(\mp\frac{1}{4}, \mp\frac{b}{2} + (-1)^{\frac{m\pm1}{2}}\frac{c}{2}\right), \quad \mathbf{z_1}^{(0,1)} = \left(\frac{a}{2} \mp \frac{1}{4}, 0\right), \quad (6)$$

as also shown in Ref. 22. If the indicator points belong to a regular orbit, they belong to the shearless curve,[30] and we can use this information to study the persistence and the breakup of the curve. The parameter space for the existence of the shearless curve is constructed by inspecting the trajectory of the indicator points.[29,30] The method consists of iterating all the indicator points for a long time interval. If the trajectory remains between a certain value of y, $|y| < 10$, the trajectory is a regular solution and the shearless curve exists in the phase space. Applying this method for each pair (a, b) and for $a \geq 0.8$, if the shearless curve exists, we plot a point in the parameter space and, if it does not, we leave it blank. The parameter spaces for $m = 1$, $m = 3$, and different values of c are shown in Fig. 3. We choose $a \geq 0.8$ due to the fact that our calculations are in this region of the parameter space.

The parameter space for the standard nontwist map (for $c = 0.000$) can be seen in Ref. 29. The parameter space for the symmetric cases for $m = 1$ of ESNM is exhibited in Figs. 3(a) and 3(b). When increasing the perturbation amplitude c, the number of points for the existence of the shearless curve decreases. The shape for $m = 1$ of the parameter space is preserved, and, for higher values of m, there is a shift of the critical curve, the boundary between the colored and the white region, for lower values of b. In a different way, for $m = 3$, the shape of the colored region for different values of c is relatively distinct. When the values of c increase, the parameter space shows an even more nontrivial structure. However, we only see a decrease in the number of points (a, b) where the shearless curve exists. The perturbation always anticipates the breakup of the shearless curve. We corroborate this observation by calculating the fraction of the region of the parameter space with the existence of the shearless curve (colored region area), as shown in Table I.

TABLE I. Fraction of the colored region of the parameter space region $a \in [0.8, 1.0]$ and $b \in [0, 1]$. The increase in the c values decreases the area corresponding to the existence of the barrier.

	$c = 0.005$	$c = 0.050$	$c = 0.100$
$m = 1$	0.42	0.37	0.32
$m = 3$	0.41	0.28	0.16

For even m, we need another strategy to determine the presence of the barriers and to estimate the critic values of a and b for the breakup of the last barrier, since for this case, the map is asymmetric and the indicator points do not exist. The method used in this work is based on the construction of escape basins in the phase space. An escape basin is defined by the set of initial conditions in the phase space that escape for a specific and previously defined exit. In a previous work, we define as exits for the standard nontwist map the lines $y = \pm 1$.[24] We use the same setup here: there are two exits **A** and **B** placed in the lines $y = 1$ and $y = -1$ and the respective escape basins for each exit is the set of initial conditions that, after some time τ, their trajectories cross the exit lines. If the trajectory does not escape until the time limit τ, we assume that the orbit is regular, an island or a barrier, or the orbit is trapped in a stickiness region.

To construct the parameter space based on the escape basin concept, we consider, for a map with $m = 2$, a grid of 1000×2000 initial conditions uniformly distributed over the region $\{[0, 1) \times (-1, 1)\}$ in the phase space. If the trajectory from an initial condition crosses $y = 1$ ($y = -1$), until $\tau = 1000$ iterations, we mark this initial point by a purple (orange) point, otherwise, the

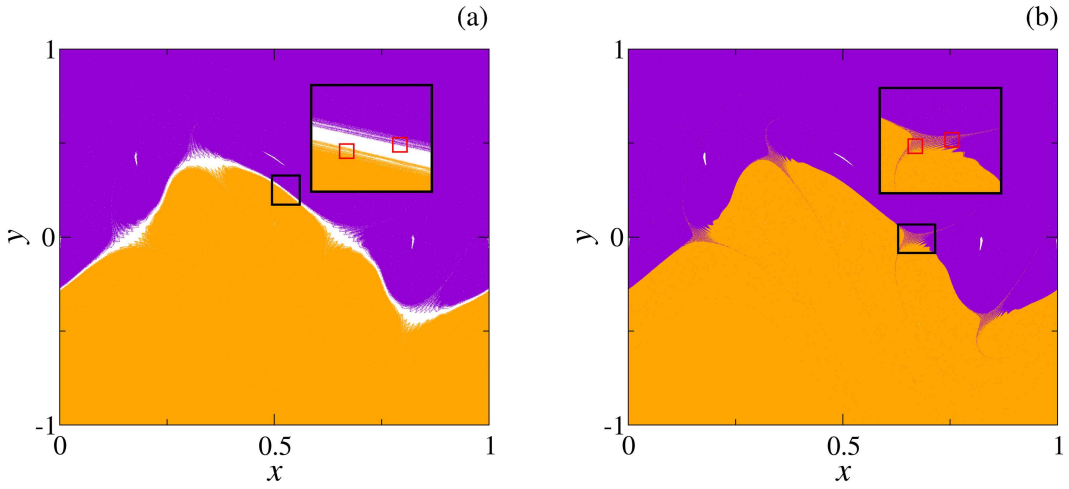

FIG. 4. Two examples of escape basins for the extended standard nontwist map. The orange (purple) points represent the initial conditions of trajectories that cross the exit lines $y = -1.0$ ($y = 1.0$) and the white points indicate regular orbits that do not escape until $n = \tau = 1000$ iterations. In (a), we have a total barrier between the two basins, and in (b), we do not see a regular region separating the two colored regions. The parameters are $a = 0.823$, $c = 0.005$, $m = 2$ in both cases and (a) $b = 0.487$ and (b) $b = 0.495$.

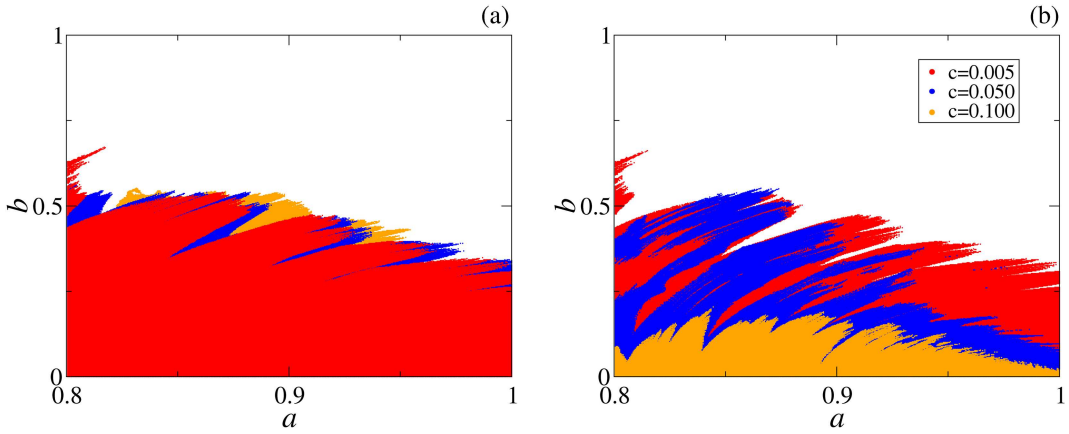

FIG. 5. Superposition of parameter spaces for the existence of a barrier in the phase space for different values of c and even values of m: (a) $m = 2$ and (b) $m = 4$.

point is left blank. In this way, the barriers in the phase space are represented by white points in the escape basin scenario. If there is a total barrier in the phase space, it would be a continuous white region between the two colored escape basins. When the barrier is broken, the two escape basins are side by side and we identify regions where the basins are connected. We see this scenario in Fig. 4 where we build the escape basins for two cases of the ESNM: (a) for a case where there is a total barrier and (b) where the barrier is missing. We observe the details of the frontier between the two basins in the magnification placed in the right corner of each figure.

To identify the absence of the white region between the two basins, as shown in Fig. 4(b), we utilize the procedure of dividing the phase space in boxes from the basin entropy evaluation.[24,31] First, we construct the escape basins as stated before and then we divide the phase space into $N_{\text{boxes}} = 200 \times 400$ boxes with 25 initial conditions in each. Then, we analyze each box searching for a configuration that indicates the mixing between the basins. If there is a barrier, we observe three cases: boxes with one color, boxes with one color and white points, as represented in the red boxes inside the magnification in Fig. 4(a), and boxes with the two colors of the basins and white points, when the barrier is narrow. When the barrier is broken, we see the same cases, where the white points can be a consequence of islands or stickiness regions. We also observe a new case, where there are boxes with the two colors and no white region between the two escape basins, as we see in Fig. 4(b). In this way, the basins share a common boundary and if we find a box with the two colors and no white points, we consider that there is no barrier in the phase space.

Following the method described above, we evaluate the space parameter for the three values of c previously indicated. For each pair (a, b), we verify if there is a barrier in the phase space, i.e., if all the boxes are in the three categories specified previously. If there is a barrier the point will be plotted, otherwise the point will be left blank. The parameter spaces for even values of m are exhibited in Fig. 5.

Observing the parameter spaces in Fig. 5, we see that the increase of the c values does not always imply a decrease in the region that represents the existence of a regular curve. In Table II, we show the area of the barrier region in the parameter space (the colored region). For $m = 2$, we see the opposite scenario for odd m. As c grows, the critical curve of the parameter space changes to higher values of b, which means that for some regions of the space the perturbation $c\sin(2\pi mx)$ postpone the break up of the last curve. For a better visualization, we invert the order of plotting the parameter spaces and bring the red space (smaller c) to the front. We cannot affirm that the last curve is the shearless curve, once there is not a confirmation that the last curve is a shearless one.[29] For $m = 4$, the scenario is similar to $m = 3$. In Fig. 3(b), the colored region decreases as the perturbation amplitude c grows, as quantified and exposed in Table II. We verify that the shape of the parameter space is not preserved. One interesting phenomenon to pint out is the nontrivial shape of the parameter space for $m = 4$ and $c = 0.050$. For this case, we have a disjointed set where we can see "holes" in the region, between $a = 0.8$ and $a = 0.85$, causing a non-unique boundary.

TABLE II. The area of the colored region of the parameter space region shown in Fig. 5. The increase in c for $m = 4$ causes a decrease in the area for the existence of a barrier. For $m = 2$, $c = 0.050$ presents an area slightly bigger than $c = 0.005$ and $c = 0.100$.

	$c = 0.005$	$c = 0.050$	$c = 0.100$
$m = 2$	0.43	0.45	0.42
$m = 4$	0.43	0.28	0.11

IV. DIRECTED TRANSPORT

As shown before, the ESNM presents a Hamiltonian ratchet in the phase space, i.e., a directed transport for the asymmetric case represented by even m. The ratchet effects are exhibited in Fig. 2(a) by the non-zero value of $\langle y \rangle$ during the time evolution. There are many methods to describe the transport properties in the system.[3] In

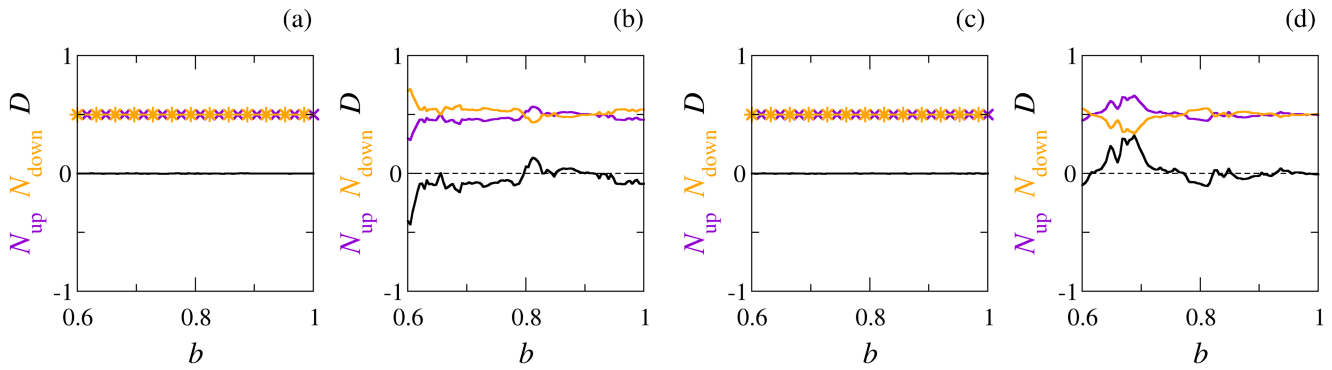

FIG. 6. Number of chaotic trajectories with initial conditions at $y = 0$ that cross $y = 1$ (N_{up} represented by the purple curve) or $y = -1$ (N_{down} represented by the orange curve) and the difference $D = N_{up} - N_{down}$ indicated by the black curve, calculated for each value of b. In this case, $a = 0.805$, $c = 0.050$, (a) $m = 1$, (b) $m = 2$, (c) $m = 3$, and (d) $m = 4$.

this work, we proposed a new method to study the directed transport in the phase space. It is similar to the transmissivity[24,32] and investigates the tendency of the trajectories goes to a specific direction in y.

To describe the tendency of the transport in the phase space, we choose 10^6 initial conditions that belong to the chaotic sea over $y = 0$ and iterate them for $n = 1000$. Then, we count how many trajectories go to the upper region of the phase space crossing the

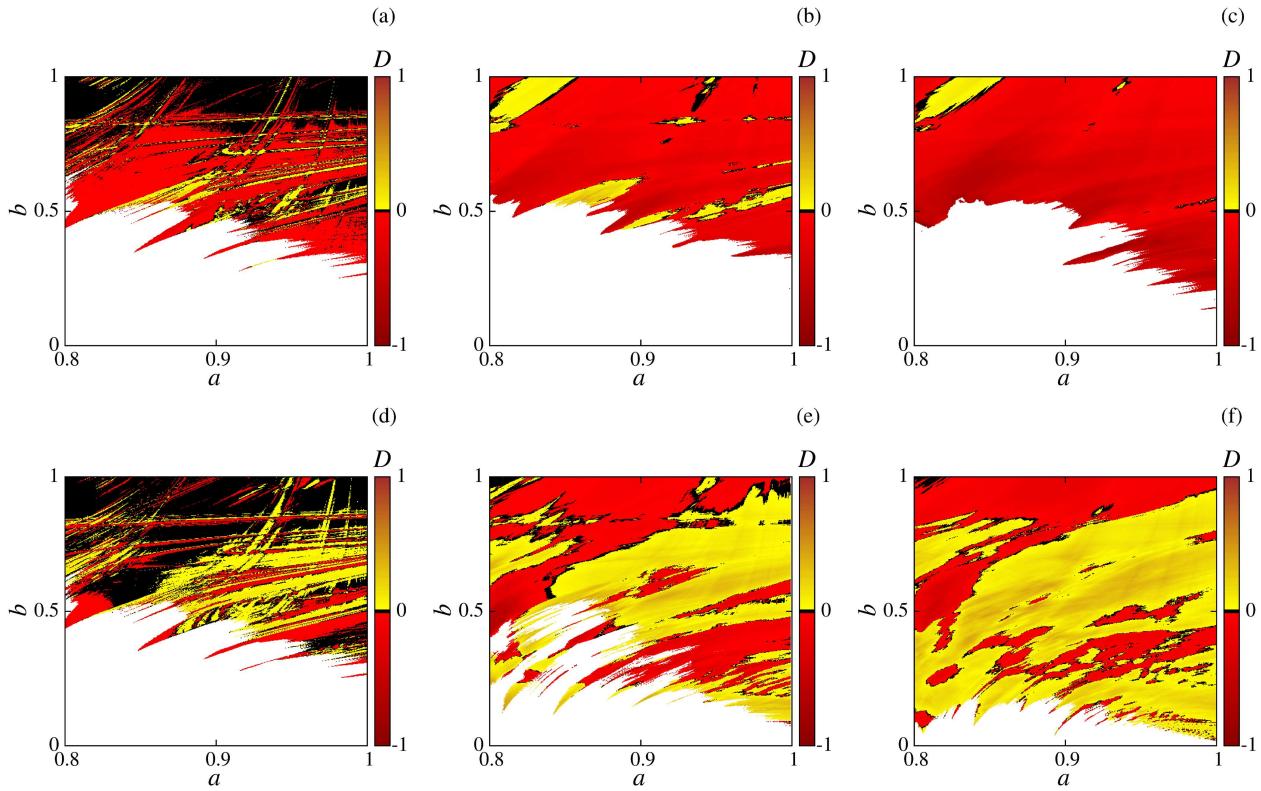

FIG. 7. Parameter space for the difference of the number of trajectories D for even m and different values of c. The yellow (red) points indicate a set of parameters (a, b) where the trajectories started in $y = 0$ tend to go upward (downward) in the phase space. The values of c and m are $c = 0.005$ for the first column, $c = 0.050$ for the second one and $c = 0.100$ for the third column. For m, we have $m = 2$ for the first upper row and $m = 4$ for the lower row.

line $y = 1$ and how many go to the lower region crossing $y = -1$ and normalize this number by the total number of trajectories. The fraction of the number of trajectories that go upward (downward) in the phase space is designated by N_{up} (N_{down}). Once we are interested in the transport tendency, we calculate the difference $D = N_{up} - N_{down}$. If $D > 0$ ($D < 0$), we have most of trajectories going to the upper (lower) region in the phase space and, consequently, a ratchet that directs the transport to the upward (downward) direction.Otherwise, if $D = 0$, we do not have a directed transport, the tendency to go to any direction is the same.

Fixing $a = 0.805$ and $c = 0.050$, we calculate N_{up}, N_{down}, and the difference D for different values of b and m. The results are shown in Fig. 6. As expected, the difference D (black curve) between the number of trajectories that go upward and downward is null for the symmetric case $m = 1$ [Fig. 6(a)] and $m = 3$ [Fig. 6(c)]. In the odd case, we have an equal tendency of the trajectories: 50% go upward ($N_{up} = 0.5$, the purple curve with purple $\times$ symbol) and 50% of the solutions go downward ($N_{down} = 0.5$, the orange curve with an orange star symbol).

A different scenario is presented for even m. For the asymmetric case, shown in Figs. 6(b) and 6(d), we see that the number of chaotic trajectories that go upward and downward oscillates around $N = 0.5$, but $N_{down} \neq N_{up}$ for almost all values of b. Therefore, there is a ratchet-like scenario in these cases.

In Fig. 6, we fix the value of a in $a = 0.805$. If we calculate the difference D for all parameter pairs (a, b) in the parameter spaces in Fig. 5, where there is no barrier, we obtain the parameter space for the directed transport, as shown in Fig. 7. In the parameter spaces shown in Fig. 7, the white region represents the pair of parameters (a, b) where there is a barrier (parameter spaces in Fig. 5). The colored regions represent three different scenarios: transport with no preferential direction (black region), upward directed transport (yellow region), and downward directed transport (red region).

For $m = 2$ in Figs. 7(a)–7(c), we see the prevalence of downward directed transport as the values of c grow. For $c = 0.005$, Fig. 7(a), there is a significant undirected transport region and a small yellow region for upward transport. When the c values grow to $c = 0.050$ and $c = 0.100$, the black region is small and is concentrated at the border of the red and yellow regions. Upward directed transport is most likely to occur at $c = 0.050$. If we increase the perturbation, we see in Fig. 7(c) that the yellow region is concentrated in a portion of the parameter space and the red regions show up, indicating the preference for downward directed transport.

In Figs. 7(d)–7(f), we compute the parameter spaces for $m = 4$ and observe the opposite scenario. The undirected transport, in this case, is also more likely to occur at small values of c, as $c = 0.005$ [Fig. 7(d)]. However, as c grows, we see the predominance of the yellow region in the parameter space. For $c = 0.050$ and $c = 0.100$, we have few black points and red regions immerse in the big yellow area. Therefore, for $m = 4$ there is a preference for the upward direction for transport.

The distribution of the colored regions is not trivial. There is no simple structure in the parameter space, so it is not possible to predict the preferential direction of the transport, it is necessary to calculate the difference for each pair (a, b). This observation corroborates with Cheon's remark that the directed transport is controllable but not predictable.[28]

V. CONCLUSIONS

In this work, we study the consequences of a new perturbation with the form $c \sin(2\pi mx)$ added to the well studied nontwist standard map. This new perturbation leads to the extended nontwist standard map (ENSM). In ESNM, we verify the existence of a symmetric and intuitive behavior when m is odd and an opposite case when the system presents itself as an asymmetric one with counterintuitive features, for even values of m.

For the odd cases, $m = 1$ and $m = 3$, the scenario of twin island chains is preserved, i.e., the two island chains are equal and the islands have the same size and inner structure. Consequently, the stickiness observed around the two chains is equivalent. One point noted in the asymmetric case, even m, is the breakup of this scenario of twin islands. The islands of different chains are not correspondent and the bifurcations of the inner curves happen at different parameters. An unbalanced stickiness is also observed in a high concentration of points in the chaotic sea around one specific island chain.

The mechanism responsible for the twin island scenario breakup is the spatial asymmetry represented by the violation of the relation between the map M and the symmetry transformation T: $TM \neq MT$. For odd m, the relationship is valid, the indicator points can be defined and the parameter space for the existence of the shearless can be constructed. The main effect of the new perturbation in the barriers in the phase space for the symmetric case is the anticipation of the breakup of the shearless curve. For higher values of amplitude c, the curve breaks for lower values of b.

Once the symmetry transformation cannot be applied in the system for even m, we proposed a new method to construct the parameter space, which is based on the analysis of the escape basins and the mixing between them. From this method, the parameter spaces for the existence of a barrier are presented as nontrivial and counterintuitive. For $m = 2$, when c grows, the number of points in the parameter spaces can also increase, as we see for $c = 0.050$. Increasing the amplitude of the perturbation can postpone the breakup of the barriers in the ESNM. For $m = 4$, we recover the intuitive phenomenon of anticipating the breakup of the barrier as c grows, but we identify a nontrivial structure in the parameter space. For $c = 0.050$, we find a disjoint set of points in the parameter space, as well as the boundary between the colored and the blank regions is more complicated and is not unique.

In the final part of our work, we study the transport in the phase space. Due to the spatial symmetry breaking, which occurs with even m, we identify a preferential direction for the chaotic trajectories to go up or down in y. Defining the difference between the fraction of trajectories that go up and down, we observe in the parameter space some regions of (a, b) where the transport has a negative preferential direction, represented by the red color in Fig. 7. This red region is dominant for $m = 2$ and vanishes for $m = 4$ as the c value increases. For $m = 4$, we see the dominance of the yellow regions that represents a preferred upward direction. In this case, the yellow region grows and the red region vanishes for higher values of c. In both cases, we observe that for some points (a, b), there is a symmetric transport and no preferential direction for the chaotic solutions. The black region (no preferential direction) is more predominant for lower values of c. This region decreases and concentrates on the

boundary between the yellow and red regions for high c. In this way, we show that the Hamiltonian ratchet effect is due to directed transport and is a possible phenomenon for this system but the direction for a set of parameters (a, b, c) is not predictable.

ACKNOWLEDGMENTS

We wish to acknowledge the support of the Araucária Foundation, National Council for Scientific and Technological Development (CNPq), Coordination for the Improvement of Higher Education Personnel (CAPES), and São Paulo Research Foundation (FAPESP) (Grant No. 2018/03211-6). We would also like to thank the 105 Group Science (www.105groupscience.com) for fruitful discussions.

DATA AVAILABILITY

The data that support the findings of this study are available from the corresponding author upon reasonable request.

REFERENCES

[1]R. S. MacKay, J. D. Meiss, and I. C. Percival, "Stochasticity and transport in Hamiltonian systems," Phys. Rev. Lett. **52**, 697 (1984).
[2]R. S. MacKay, J. D. Meiss, and I. C. Percival, "Transport in Hamiltonian systems," Physica D **13**, 55–81 (1984).
[3]G. Boffetta, G. Lacorata, G. Redaelli, and A. Vulpiani, "Detecting barriers to transport: A review of different techniques," Physica D **159**, 58–70 (2001).
[4]M. F. Carusela, A. J. Fendrik, and L. Romanelli, "Transport and dynamical properties of inertial ratchets," Physica A **388**, 4017–4024 (2009).
[5]J. Gong and P. Brumer, "Directed anomalous diffusion without a biased field: A ratchet accelerator," Phys. Rev. E **70**, 016202 (2004).
[6]I. Dana and V. B. Roitberg, "Weak-chaos ratchet accelerator," Phys. Rev. E **83**, 066213 (2011).
[7]N. A. C. Hutchings, M. R. Isherwood, T. Jonckheere, and T. S. Monteiro, "Chaotic Hamiltonian ratchets for pulsed periodic double-well potentials: Classical correlations and the ratchet current," Phys. Rev. E **70**, 036205 (2004).
[8]A. Celestino, C. Manchein, H. A. Albuquerque, and M. W. Beims, "Ratchet transport and periodic structures in parameter space," Phys. Rev. Lett. **106**, 234101 (2011).
[9]S. Denisov, J. Klafter, M. Urbakh, and S. Flach, "DC currents in Hamiltonian systems by Lévy flights," Physica D **170**, 131–142 (2002).
[10]E. Neumann and A. Pikovsky, "Quasiperiodically driven Josephson junctions: Strange nonchaotic attractors, symmetries and transport," Eur. Phys. J. B **26**, 219–228 (2002).
[11]M. Vlad, F. Spineanu, and S. Benkadda, "Impurity pinch from a ratchet process," Phys. Rev. Lett. **96**, 085001 (2006).
[12]A. B. Schelin and K. H. Spatschek, "Directed chaotic transport in the tokamap with mixed phase space," Phys. Rev. E **81**, 016205 (2010).
[13]C. Mennerat-Robilliard, D. Lucas, S. Guibal, J. Tabosa, C. Jurczak, J.-Y. Courtois, and G. Grynberg, "Ratchet for cold rubidium atoms: The asymmetric optical lattice," Phys. Rev. Lett. **82**, 851 (1999).
[14]P. Reimann, M. Grifoni, and P. Hänggi, "Quantum ratchets," Phys. Rev. Lett. **79**, 10 (1997).
[15]L. Wang, G. Benenti, G. Casati, and B. Li, "Ratchet effect and the transporting islands in the chaotic sea," Phys. Rev. Lett. **99**, 244101 (2007).
[16]D. del Castillo-Negrete, J. M. Greene, and P. J. Morrison, "Area preserving nontwist maps: Periodic orbits and transition to chaos," Physica D **91**, 1–23 (1996).
[17]D. del Castillo-Negrete and P. J. Morrison, "Chaotic transport by Rossby waves in shear flow," Phys. Fluids A Fluid Dyn. **5**, 948–965 (1993).
[18]P. J. Morrison, "Magnetic field lines, Hamiltonian dynamics, and nontwist systems," Phys. Plasmas **7**, 2279–2289 (2000).
[19]I. Caldas, R. Viana, J. Szezech, J. Portela, J. Fonseca, M. Roberto, C. Martins, and E. da Silva, "Nontwist symplectic maps in tokamaks," Commun. Nonlinear Sci. Numer. Simul. **17**, 2021–2030 (2012).
[20]A. Haro and R. de la Llave, "Efficient and reliable algorithms for the computation of non-twist invariant circles" (unpublished).
[21]J. S. E. Portela, I. L. Caldas, R. L. Viana, and P. J. Morrison, "Diffusive transport through a nontwist barrier in tokamaks," Int. J. Bifurc. Chaos **17**, 1589–1598 (2007).
[22]A. Wurm and K. M. Martini, "Breakup of inverse golden mean shearless tori in the two-frequency standard nontwist map," Phys. Lett. A **377**, 622–627 (2013).
[23]J. M. Greene and J. Mao, "Higher-order fixed points of the renormalisation operator for invariant circles," Nonlinearity **3**, 69 (1990).
[24]M. Mugnaine, A. C. Mathias, M. S. Santos, A. M. Batista, J. D. Szezech, Jr., and R. L. Viana, "Dynamical characterization of transport barriers in nontwist Hamiltonian systems," Phys. Rev. E **97**, 012214 (2018).
[25]J. D. Szezech, Jr., I. L. Caldas, S. R. Lopes, P. J. Morrison, and R. L. Viana, "Effective transport barriers in nontwist systems," Phys. Rev. E **86**, 036206 (2012).
[26]J. D. Szezech, Jr., I. L. Caldas, S. R. Lopes, R. L. Viana, and P. J. Morrison, "Transport properties in nontwist area-preserving maps," Chaos **19**, 043108 (2009).
[27]S. R. Lopes, J. D. Szezech Jr., R. F. Pereira, A. A. Bertolazzo, and R. L. Viana, "Anomalous transport induced by nonhyperbolicity," Phys. Rev. E **86**, 016216 (2012).
[28]T. Cheon, P. Exner, and P. Šeba, "Extended standard map with spatio-temporal asymmetry," J. Phys. Soc. Jpn. **72**, 1087–1091 (2003).
[29]A. Wurm, A. Apte, and P. J. Morrison, "On reconnection phenomena in the standard nontwist map," Braz. J. Phys. **34**, 1700–1706 (2004).
[30]S. Shinohara and Y. Aizawa, "Indicators of reconnection processes and transition to global chaos in nontwist maps," Prog. Theor. Phys. **100**, 219–233 (1998).
[31]A. Daza, A. Wagemakers, B. Georgeot, D. Guéry-Odelin, and M. A. Sanjuán, "Basin entropy: A new tool to analyze uncertainty in dynamical systems," Sci. Rep. **6**, 31416 (2016).
[32]I. L. Caldas, R. L. Viana, C. V. Abud, J. C. D. Fonseca, Z. O. Guimarães Filho, T. Kroetz, F. A. Marcus, A. B. Schelin, J. D. Szezech Jr, D. L. Toufen *et al.*, "Shearless transport barriers in magnetically confined plasmas," Plasma Phys. Control. Fusion **54**, 124035 (2012).